The 1979 Extractive Metallurgy Lecture
The Metallurgical Society of AIME

Thermodynamic Evaluations of Extractive Metallurgical Processes

AKIRA YAZAWA

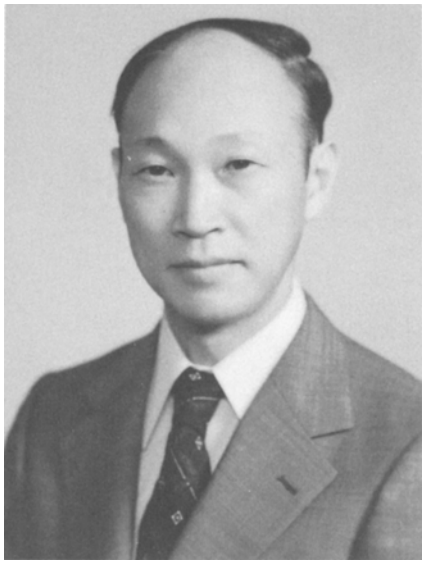

Among the various, possible applications of thermodynamics to extractive metallurgical processes, the availability of chemical potential diagrams and calculation methods combining stoichiometric relations with equilibrium constants are emphasized. In hydrometallurgical processes, the value of potential-pH diagrams has been well recognized and the application of similar techniques to rather complex systems containing ligands such as the cyanidation process is very interesting. In the roasting of sulfide ores, various information is derived from sulfur-oxygen potential (log p_{S_2} –log p_{O_2}) diagrams. Especially convenient for sulfation roasting are the SO_2-O_2 potential diagrams. Various smelting processes including the direct production of metal from sulfide ore are discussed with the use of chemical potential diagrams. Based upon the prediction derived from sulfur-oxygen potential diagram, the recovery of elemental sulfur from oxidation of FeS is evaluated by stoichiometric calculations. Volatilization behavior of elements such as zinc, cadmium, and mercury are also explained by similar diagrams and the possibility of the direct distillation of zinc sulfide is predicted by stoichiometric calculations. Analogous calculations are used to clarify the reasons why the segregation process is amenable to copper oxide ore but not to nickel ore.

THERMODYNAMICS has wide applicability in the field of extractive metallurgy. However, this discipline has not been accepted by industrial engineers as widely as might have been hoped. Recently, a considerable number of researchers has directed their efforts to bridge this gap between fundamental theories and practical processes.

Various thermodynamic techniques have been developed to evaluate practical problems and to estimate optimum conditions. In this paper, the effectiveness of chemical potential diagrams and stoichiometric calculations incorporating equilibrium constants are emphasized. Both methods are not new but very useful especially for evaluating optimum conditions in complex operations and for predicting the possibility of new processes.

The Extractive Metallurgy Lecture was authorized in 1959 to provide an outstanding man in the field of nonferrous metallurgy as a lecturer at the annual AIME meeting.

AKIRA YAZAWA is a Professor at the Research Institute of Mineral Dressing and Metallurgy of Tohoku University in Japan. He also serves as Head of the Laboratory of Environmental Chemistry there. He was educated at Tohoku University, graduating in 1948.

Mr. Yazawa began his career in 1953 as Assistant Professor in the Department of Metallurgy, Faculty of Engineering at Tohoku University. In 1963 he became Professor, Division of Pyrometallurgy at the Research Institute of Mineral Dressing and Metallurgy at Tohoku. He is the author of eighty papers and the text, *Hydrometallurgy and Waste Water Treatment.*

Mr. Yazawa is the recipient of three awards: the 1965 Meritorious Award and 1979 Tanigawa-Harris Award from the Japan Institute of Metals and the 1978 Best Paper Award from the Mining and Metallurgical Institute of Japan. His fields of research include: heterogenous equilibria in copper smelting systems; thermodynamic studies of metallurgical liquid phases; and environmental chemistry in extractive metallurgy.

ISSN 0360-2141/79/0911-0307$00.75/0

An excellent general description of chemical potential diagrams is given by Masuko.[1] The chemical potential of a given component is generally expressed as:

$$\mu_i = \mu_i^o + RT \ln a_i \quad [1]$$

thus, log a_i corresponds to a chemical potential at a definite temperature. For the reaction in the metal-oxygen system,

$$2\,M(s) + O_2 = 2\,MO(s) \quad [2]$$

when the condensed phase activities are unity,

$$\Delta G^o = A + BT = RT \ln p_{O_2} \quad [3]$$

The right side of Eq. [3], $RT \ln p_{O_2}$, is termed the oxygen potential and is proportional to log p_{O_2} at a given temperature. It is well understood from Eq. [3] that log p_{O_2} *vs* $1/T$ diagrams and even the Ellingham diagram are renditions of chemical potential diagrams. The applicability of such simple diagrams is well recognized. Thus, only the more complex systems will be treated in this paper with the occasional use of stoichiometric calculations.

HYDROMETALLURGY

A well known example of chemical potential is pH or $-\log a_{H^+}$ which defines the hydrogen ion potential in an aqueous solution. To choose a simple example, the hydrolysis equilibria,

$$M^{2+} + 2\,H_2O = M(OH)_2 + 2\,H^+ \quad [4]$$

$$\log K_4 = 2 \log a_{H^+} - \log a_{M^{2+}} = -2\,pH - \log a_{M^{2+}} \quad [5]$$

is calculated based upon the data compiled by this author,[2] and is illustrated by plotting log $a_{M^{2+}}$ *vs* pH to construct the chemical potential diagram, as shown in Fig. 1. This figure can be applied to explain leaching, purification, or waste water treatment.

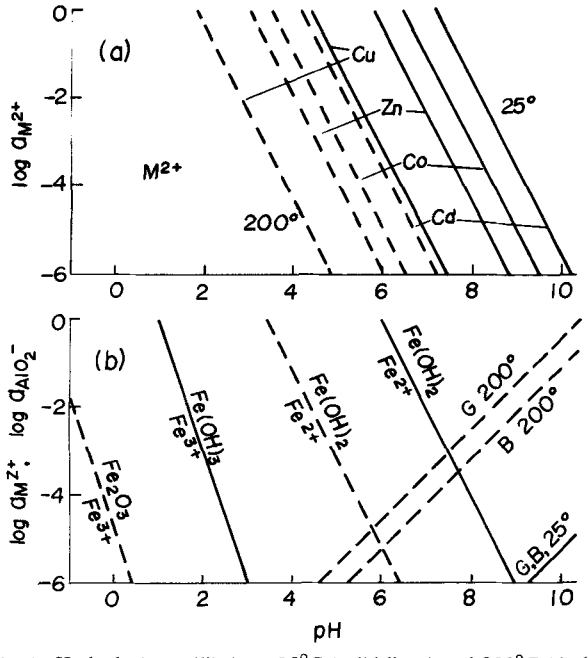

Fig. 1—Hydrolysis equilibria at 25°C (solid lines) and 200°C (dashed line).

As indicated in Fig. 1, a shift to the left of up to 3 *p*H units occurs in the hydrolysis lines when the temperature is increased from 25 to 200°C. An even larger shift in *p*H value occurs in the dehydration of the hydroxide into oxide. In the solution purification process at ordinary temperatures, it is well known that ferric ions but not ferrous ions are separable from nonferrous ions by precipitation at *p*H 2 to 4. At 200°C, precipitation of the ferric ion is accomplished even in more strongly acidic solutions. In considering the reverse reaction of the leaching of oxides, the selective separation of the nonferrous species from iron oxide can easily be realized at 200°C by the use of strong acids. However, it may be difficult to carry out the same leaching process at room temperature because weak acids in the *p*H 2 to 4 range must be used. These principles are widely accepted in various metallurgical processes and can easily be illustrated by referring to log $a_{M^{2+}}$ *vs* *p*H, chemical potential diagrams.

The simplified, basic reactions of the Bayer Process are as follows:

$$\text{for Gibbsite: } Al(OH)_3 + OH^- = AlO_2^- + 2\,H_2O \quad [6]$$

$$\text{for Boehmite: } AlOOH + OH^- = AlO_2^- + H_2O \quad [7]$$

These equilibria are represented in Fig. 1(*b*) according to the data given by Russell *et al.*[3] The horizontal axis, *p*H, varies with temperature according to Eq. [8],

$$pH_{200} = pH_{25} \cdot K_{w_{25}}/K_{w_{200}} = 0.805\,pH_{25} \quad [8]$$

where K_w is the dissociation constant of water. Accounting for this effect, caustic leaching is still easily achieved at high temperature. Moreover, as shown in Fig. 1(*b*), it is easier to leach gibbsite than boehmite at 200°C, while at 25°C, no significant difference exists. Undoubtedly, the application of increased temperatures in the Bayer Process is primarily based on kinetic aspects. However, invaluable contributions are derived from a thermodynamic examination.[2]

The Eh-*p*H diagram for aqueous solution systems is well understood and can be established also at elevated temperatures in connection with the above discussion. In this case, "potential" refers to the potential of electrons and suggests the degree of oxidation or reduction. The application of Eh-*p*H diagrams to evaluate sulfide leaching processes is excellently summarized by Peters.[4]

The utilization of similar techniques to rather complex aqueous systems containing ligands is very interesting and is described by Masuko.[5] Following his description, results based upon the data compiled by Sillen[6] and Latimer[7] are illustrated in Fig. 2 in order to explain the cyanidation process. Based upon the following data,

$$Au^+ + e^- = Au \quad E = 1.68 + 0.0591 \log a_{Au^+} \quad [9]$$

$$Ag^+ + e^- = Ag \quad E = 0.80 + 0.0591 \log a_{Ag^+} \quad [10]$$

both gold and silver are very stable. However, if the activities of Au^+ and Ag^+ can be reduced to extremely low levels, the potential, E, may decrease to a level where the metals can be placed into solution.

In the cyanide solution, the complexing reactions,

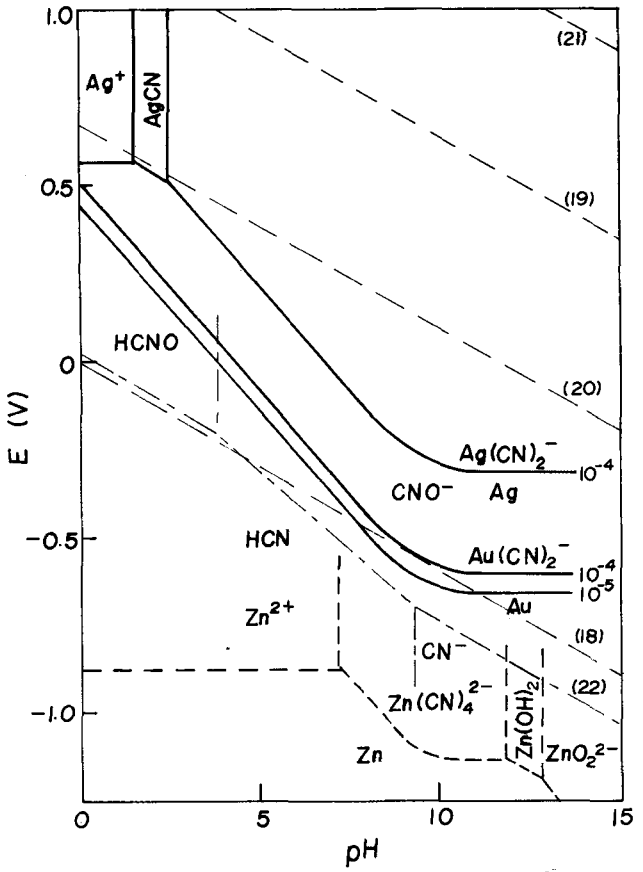

Fig. 2—Potential–*p*H diagram for cyanidation process at 25°C under 10^{-2} of the total cyanide content.

$$Au^+ + 2\ CN^- = Au(CN)_2^- \qquad [11]$$

$$p\text{CN} = 19 + 0.5 \log a_{Au^+}/a_{Au(CN)_2^-}$$

and,

$$Ag^+ + 2\ CN^- = Ag(CN)_2^- \qquad [12]$$

$$p\text{CN} = 9.4 + 0.5 \log a_{Ag^+}/a_{Ag(CN)_2^-}$$

occur and indicate that the concentration of Ag^+ may be one hundred times smaller than that of the $Ag(CN)_2^-$ ion and that the amount of Ag^+ is negligible when the value of a_{CN^-} is $10^{-8.4}$. The dissolution reactions of gold and silver are:

$$Au(CN)_2^- + e^- = Au + 2\ CN^- \qquad [13]$$

$$E = -0.60 + 0.118\ p\text{CN} + 0.0591 \log a_{Au(CN)_2^-}$$

and,

$$Ag(CN)_2^- + e^- = Ag + 2\ CN^- \qquad [14]$$

$$E = -0.31 + 0.118\ p\text{CN} + 0.0591 \log a_{Ag(CN)_2^-}$$

In addition, the occurrence of the reaction,

$$H^+ + CN^- = HCN,\ p\text{H} + p\text{CN} = 9.4 - \log a_{HCN} \qquad [15]$$

results in considerable cyanide loss through the formation of the species, HCN, when the pH falls below the value of 9.4. The total cyanide content, A, referred to in practice is defined by the following equation,

$$A = a_{HCN} + a_{CN^-} \qquad [16]$$

and Eq. [15] becomes:

$$p\text{H} + p\text{CN} = 9.4 - \log A + \log (1 + 10^{p\text{H} - 9.4}) \qquad [17]$$

By combining Eq. [17] with [13] or [14], the dissolution equliibria of gold or silver can be illustrated in an Eh-*p*H diagram.

Figure 2 is thus constructed with A equal to 10^{-2} which corresponds approximately to a 0.05 pct NaCN content. The activities of $Au(CN)_2^-$ and $Ag(CN)_2^-$ are set at 10^{-4} which closely corresponds to a silver and gold concentration of 10 and 20 g/m^3, respectively. The line representing an activity of 10^{-5} for the gold cyanide anion is also included. The above conditions closely agree with those found in practical operations.

From Fig. 2, one can easily recognize that gold and silver are very noble in the low *p*H region but become less noble in high *p*H, cyanide solutions. Notably, silver is much more inert than gold in the presence of cyanide.

The oxidation Eqs. [13] and [14] involve the release of electrons which in turn must be accepted by one of the following reducing reactions:

$$2\ H^+ + 2\ e^- = H_2 \qquad [18]$$

$$O_2 + 4\ H^+ + 4\ e^- = 2\ H_2O \qquad [19]$$

$$O_2 + 2\ H^+ + 2\ e^- = H_2O_2 \qquad [20]$$

$$H_2O_2 + 2\ H^+ + 2\ e^- = 2\ H_2O \qquad [21]$$

These equilibria are illustrated in Fig. 2 assigning unit activities to H_2O_2 and the gaseous species. The evolution of hydrogen according to Eq. [18] seems to be difficult except for limited conditions in the extraction of gold. Many researchers have confirmed that the dissolution of gold and silver is accompanied by the production of hydrogen peroxide and thus, Eq. [20] must serve as the reducing reaction.

However, Kameda[8] and Lund[9] pointed out that strong oxidizing agents such as H_2O_2 can convert CN^- into cyanate ions and this CNO^- is not capable of oxidizing gold or silver. Thermodynamic calculations also suggest that CNO^- hardly forms complex ion such as $Ag(CNO)_2^-$ or $Ag(CN)_2^-$ in the region convenient for the dissolution of silver. Theoretically, the conversion equilibrium between cyanide and cyanate ions,

$$CNO^- + 2\ H^+ + 2\ e^- = CN^- + H_2O \qquad [22]$$

$$E = -0.141 - 0.0591\ p\text{H} + 0.0296 \log a_{CNO^-}/a_{CN^-}$$

possesses a relatively low potential, as shown in Fig. 2. However, experience in cyanide waste water treatment suggests that a considerable over potential is necessary to enable Eq. [22] to proceed to the left. Therefore, the CN^- ion is stable in the region where the reactions represented by Eqs. [13] and [14] take place. Such difference of practical observation from thermodynamic evaluation is sometimes observed especially in hydrometallurgical processes. Finally, the CN^- ion will not be stable if Eqs. [19] and [21] occur due to the high location of these equilibria and it would not be thermodynamically rational to couple these equilibria with Eqs. [13] or [14].

From Fig. 2, it can be determined that the most favorable *p*H for dissolution of gold and silver is 9.4. However, to reduce the HCN losses described earlier, a *p*H value in excess of 10.5 is usually preferred in practice.

The dissolution relation,

$$Zn(CN)_4^{2-} + 2\ e^- = Zn + 4\ CN^- \quad [23]$$

is also plotted in Fig. 2 because cementation with Zn is commonly used to recover both gold and silver. As indicated by the relatively stable location of this equilibrium potential, zinc can readily displace gold and silver from the solution to the metallic state. Because zinc wastefully reacts with dissolved oxygen, an oxygen removal step is included prior to cementation.

SULFUR-OXYGEN POTENTIAL DIAGRAM

The oxygen potential, an indispensable, basic parameter in most pyrometallurgical processes, is just one chemical potential to be controlled in the reduction of oxides. However, to evaluate the more complex processes found in sulfide and chloride metallurgy, two or more chemical potentials must be considered, analogous to the Eh-*p*H diagram in hydrometallurgy.

The fundamental reactions in sulfide metallurgy may be written as:

$$2\ M + O_2 = 2\ MO \quad [24]$$

$$\log K_{24} = 2 \log (a_{MO}/a_M) - \log p_{O_2}$$

$$2\ M + S_2 = 2\ MS \quad [25]$$

$$\log K_{25} = 2 \log (a_{MS}/a_M) - \log p_{S_2}$$

Combining both reactions,

$$2\ MS + O_2 = 2\ MO + S_2 \quad [26]$$

$$\log K_{26} = 2 \log (a_{MO}/a_{MS}) - \log p_{O_2} + \log p_{S_2}$$

Assuming that the condensed phase activities are all unity or equal to each other, the above relations for 1027°C are illustrated in Fig. 3 by the use of oxygen and sulfur potentials. In this paper, the free energy data compiled by Coughlin,[10] Richardson *et al*,[11] and Kellogg[12] are used for the oxides, sulfides, and sulfates, respectively. The stable areas for the metal, oxide, or sulfide phases are classified in this diagram. Metals confined to the stable region at the bottom left are less noble, and therefore are generally more difficult to extract.

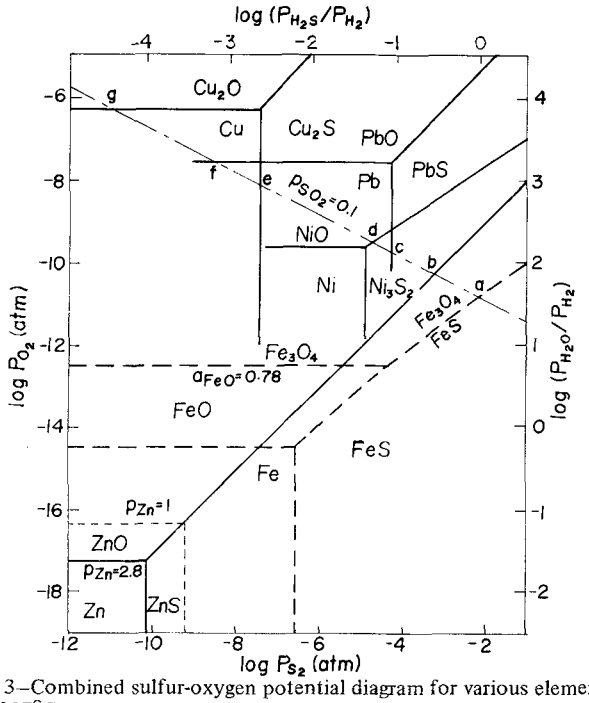

Fig. 3—Combined sulfur-oxygen potential diagram for various elements at 1027°C.

Although the lines shift according to the above equations when the condensed phase activities differ, the relative relations can be discussed on the basis of this diagram. The equilibrium partial pressures of species such as SO, SO_2, or SO_3 also can be expressed with inclined, straight lines based upon the following types of relationship:

$$1/2\ S_2 + O_2 = SO_2 \quad [27]$$

$$\log K_{27} = \log p_{SO_2} - 1/2 \log p_{S_2} - \log p_{O_2}$$

In this manner, the 0.1 atm isobar for SO_2 is illustrated in Fig. 3.

Traversing this diagram from top to bottom corresponds to the extraction of metal by reduction of oxide, a process familiar to mankind since ancient times. Similarly, an horizontal shift from right to left may be considered to obtain metal from its sulfide ore. This path is theoretically possible by reduction with hydrogen, but hardly practical due to the poor strength of the reaction and economic factors. Through long experience, man has learned that it is better to oxidize the sulfide along the line corresponding to a p_{SO_2} of 0.1 atm and then reduce to produce metal. To evaluate the various sulfide oxidation processes, the sulfur-oxygen potential diagram is very useful as shown in the following discussions.

To describe the equilibrium relations in the metal-sulfur-oxygen system, similar but somewhat different style potential diagrams have also been used, and interesting explanations were recently given by Rosenqvist.[13]

ROASTING OF SULFIDE ORES

The sulfur-oxygen potential diagram is simple in nature and easily understood when the activities of the participating condensed phases are unity, as often observed in the roasting of sulfides. As an example, the potential diagram for the Cu-S-O system at 680°C is presented in Fig. 4. The following explanation of the figure highlights the advantages of this style of chemical potential diagram:

1) The stable regions and the conditions required for each species can be grasped at a glance. The participating species are arranged in order of their oxygen or sulfur potentials. With increasing oxygen potential, the order is Cu → Cu_2O → CuO → CuO ·$CuSO_4$ → $CuSO_4$. In accordance with increasing sulfur potential, the sequence is Cu → Cu_2S → CuS. In fact, CuS is metastable at this temperature because liquid sulfur appears at a log p_{S_2} value of approximately 0.5.

2) Isobaric conditions for SO_2 and SO_3, (also SO if necessary), are represented by inclined, straight lines. Thus, equilibrium partial pressures of all the important gas species can easily be evaluated at any point in the figure. The summation of the resultant gas species from the reaction between oxygen and the sulfide,

$$p_{\Sigma O} = p_{O_2} + p_{SO_2} + p_{SO_3}, \text{ (including } p_{S_2} \text{ if necessary)} \quad [28]$$

is convenient when evaluating the oxidation reaction. The region where the value of $p_{\Sigma O}$ exceeds 1 atm cannot be considered under the normal pressure condition.

3) A reasonable reaction process can be predicted in connection with practice. Roasting with air may be approximated by following the isobars corresponding to P_{SO_2} values of 0.1 and 0.2 atm or more exactly, to $P_{\Sigma O}$ values of 0.1 to 0.2 atm. Thus, according to Fig. 4, the roasting sequence is $Cu_2S \rightarrow Cu \rightarrow Cu_2O \rightarrow CuO \rightarrow CuO \cdot CuSO_4 \rightarrow CuSO_4$. The formation of Cu metal or CuO at this temperature delicately hinges on the value of $P_{\Sigma O}$; but as already shown in Fig. 3, metallic copper is quite stable particularly when compared with other metals. In typical roaster gases containing several percent of SO_2 and O_2, the final product is $CuSO_4$. A previous controversy as to whether sulfate formed directly from the sulfide or indirectly with an intermediate MO formation stage is readily clarified by examining the diagram. Direct formation of sulfate is observed only at low temperatures for sulfate stable elements such as lead and cadmium.

4) Thermodynamically valid reactions can be distinguished from the figure. As an example, the equilibrium between Cu_2S and CuO can be expressed in the form of an equation and the free energy change and equilibrium constant derived. However, judging from the potential diagram, Cu_2S cannot change directly to CuO.

5) As will be shown in later figures, partial pressures or activities in condensed phases can be illustrated in the diagram. Accordingly, systems involving solutions or volatile components may be treated.

6) Ideas for new processes can be obtained by examining chemical potential diagrams. Apart from practical adaptability, direct sulfation of Cu_2S to $CuSO_4$ is possible in a high pressure roaster. Although less attractive practically, a second alternative would be to roast directly to copper in a single step by precisely controlling the sulfur and oxygen potentials.

In Fig. 5 is presented the 680°C diagram for the Fe-S-O system. Differing from the previous case, solid solutions of wustite and pyrrhotite are present. At this temperature, the decomposition sulfur pressure of pyrite to pyrrhotite is nearly 1 atm. At point "A", FeS is oxidized to Fe_3O_4 and the final stable product upon further oxidation is Fe_2O_3, not sulfate. The formation of metallic iron or wustite is hardly likely. It

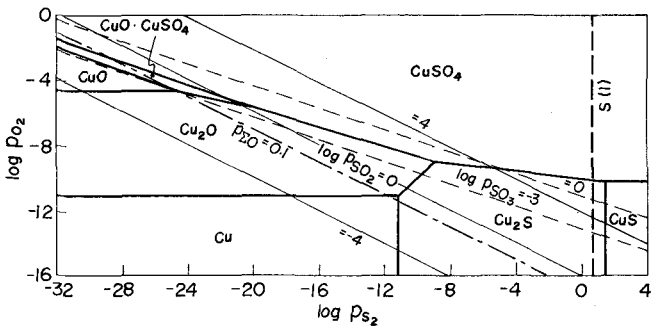

Fig. 4—Sulfur-oxygen potential diagram fro Cu-S-O system at 680°C.

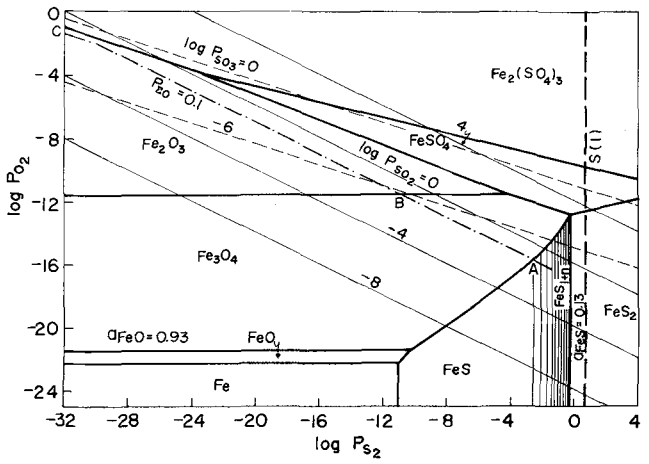

Fig. 5—Sulfur-oxygen potential diagram for Fe-S-O system at 680°C.

should be noted that FeS in the solid state is directly oxidized to magnetite.

It is well known that iron and copper share similar affinities for sulfur; but in comparing Fig. 4 with Fig. 5, iron is much less noble than copper with respect to oxygen. These relative comparisons can be conveniently performed by utilizing the overlapped diagram already shown in Fig. 3. When roasting proceeds at a p_{SO_2} of 0.1 atm, the first oxidation product is Fe_3O_4 followed by ZnO. Then, PbS, Ni_3S_2, and Cu_2S are also oxidized. In the case of PbS and Cu_2S, the metallic phase forms and is subsequently oxidized. In practical roasting operations, similar phenomena are observed. However, the formation of ferrites is well known and these complex components must be accounted for in the overlapped potential diagram.

A sulfur-oxygen potential diagram constructed for the Cu-Fe-S-O system at 827°C is presented in Fig. 6 and includes additional data on ferrite formation.[13,14] In this figure, solid solutions are punctuated by single quotation marks and their mutual boundaries are plotted based on equal activities of the condensed phases. Assuming a charge consisting of $CuFeS_2$ with small quantities of FeS, roasting under insufficient oxygen at any temperature results in the formation of Fe_3O_4 and a bornite solid solution. This step corresponds to the practice of partial roasting of copper concentrate. Quite differently, the products of a dead roast in excess oxygen vary widely with temperature; and are $CuFe_2O_4$ and CuO at 827°C, $CuFeO_2$ and $CuFe_2O_4$ at 1000°C, and $CuSO_4$ and Fe_2O_3 at 680°C.

SELECTIVE SULFATION ROASTING

Copper sulfate and hematite are the final roaster products at 680°C, as observed in Fig. 4 and 5. Therefore, this temperature appears to be suitable for selective sulfation roasting in which the nonferrous values are converted to water soluble sulfates while the iron is oxidized to insoluble hematite. Several investigators[15,16] have used log p_{SO_2} – log p_{O_2} diagrams for examination of sulfide roasting processes and this style of potential diagram is especially suited for discussing sulfation roasting. The following fundamental reactions,

$$MO + SO_3 = MSO_4 \quad \log K_{29} = -\log p_{SO_3} \quad [29]$$

$$SO_2 + 1/2\ O_2 = SO_3 \quad \log K_{30}$$
$$= \log p_{SO_3} - \log p_{SO_2} - 1/2 \log p_{O_2} \quad [30]$$

are considered in Fig. 7 in which the equilibria at 680°C are plotted as solid lines while dash-dot lines and broken lines represent the equilibria at 630 and 730°C, respectively. All lines parallel to the SO_3 partial pressure isobars express equilibria between two solid phases and illustrate the comparative stabilities of the sulfates. The stable field for the oxide is located on the left while the right side is the sulfate stability field. Although roaster gas in practical sulfation processes contains nearly 10 pct SO_2 and a few pct of O_2 such that the value of $p_{\Sigma O}$ is approximately 0.1, curves representing $p_{\Sigma O}$ values of 0.1 and 0.2 are included in Fig. 7.

At 680°C, the $Fe_2(SO_4)_3$-Fe_2O_3 equilibrium lies on the right of the $p_{\Sigma O}$ curves while the majority of the other oxide-sulfate lines are located to the left at higher p_{SO_2} values. Therefore, selective sulfation can be accomplished.

However, at 630°C, iron is also sulfated at the most probable gas composition range and selective sulfation can not be achieved. At 730°C, although iron is oxidized to insoluble Fe_2O_3, $CuSO_4$ decomposes to a basic sulfate and $ZnSO_4$ is also unstable. Since the basic sulfates, $CuO \cdot CuSO_4$ and $ZnO \cdot 2ZnSo_4$, are less soluble, the extraction of copper and zinc by acid dissolution will decrease if sulfation is carried out at 730°C. Thus, the most suitable temperature for selective sulfation is between 670 and 680°C with an allowable fluctuation of ±30°C only. These thermodynamic observations agree very well with practical experiences.[17,18] This excellent agreement at these moderate temperatures in a gas-solid reaction system indicates adequate reaction speeds and should greatly encourage the extractive metallurgist who intends to apply equilibrium theories to actual problems. At the same time it should be noticed that such selective sulfation processes could never be realized without the use of a fluidized bed roaster.

Based upon the above discussions, the optimum conditions for selective sulfation are found. However, the chemical potentials or partial pressures alone do not provide the relative quantities of the reactants necessary for engineers to determine the practical operating conditions. To fulfill this demand, stoichiometric calculations combined with thermodynamic data are very useful especially due to recent developments in computer applications.

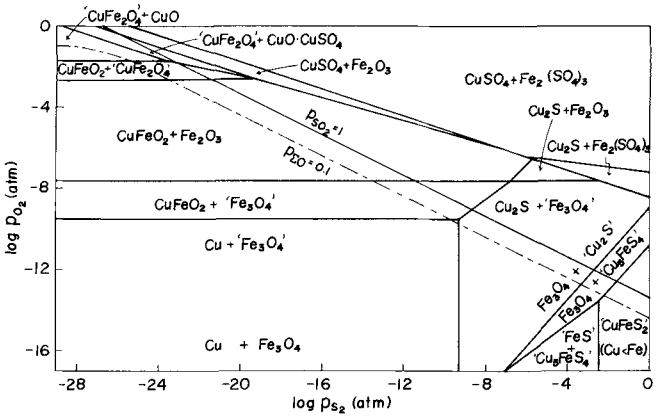

Fig. 6—Sulfur-oxygen potential diagram for Cu-Fe-S-O system at 827°C.

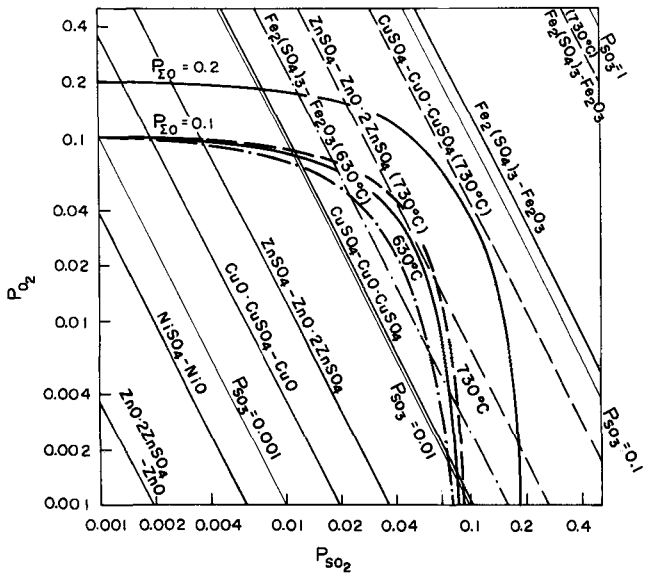

Fig. 7—SO_2-O_2 potential diagram for explaining selective sulfation roasting. Solid line: 680°C, dashed line: 730°C, dash-dot line: 630°C.

Calculations of this type were used by Kellogg[19] to explain sulfation roasting. In this paper, the roasting of copper-nickel concentrate is treated as a simple example to gain a better understanding of the process. One kilogram of concentrate with the composition given in Table I is roasted with m moles of air containing 20.7 pct O_2. The condensed phase products are $CuSO_4$, $NiSO_4$, and Fe_2O_3 while the gaseous phase is constituted of SO_2, SO_3, O_2, N_2, and H_2O. The materials balance in which n is the molar quantity of each gaseous species is as follows:

$$\text{S balance: } 10.92 = n_{SO_2} + n_{SO_3} + 1.57 + 0.85 \quad [31]$$

$$\text{O balance: } 2 \times 0.207\ m = 2\ n_{SO_2} + 3\ n_{SO_3} + 2\ n_{O_2} + 4 \times 1.57 + 4 \times 0.85 + 1.5 \times 6.27 \quad [32]$$

The total moles of gaseous product, n_T, is:

$$n_T = n_{SO_2} + n_{SO_3} + n_{O_2} + 0.793\ m + 8.33 \quad [33]$$

The equilibrium constant for Eq. [30] is expressed as follows under a one atm roasting condition:

$$K = (n_{SO_3} \cdot n_T^{1/2})/(n_{SO_2} \cdot n_{O_2}^{1/2}) \quad [34]$$

Combining Eqs. [31] to [34], the molar quantities, n_{SO_2}, n_{SO_3}, n_{O_2}, and n_T are calculated for given values of m and temperature.

Table I. Composition of Feed for Selective Sulfation Roasting

	Cu	Ni	Fe	S	H_2O
Wt Pct	10	5	35	35	15
Moles in 1 kg	1.57	0.85	6.27	10.92	8.33

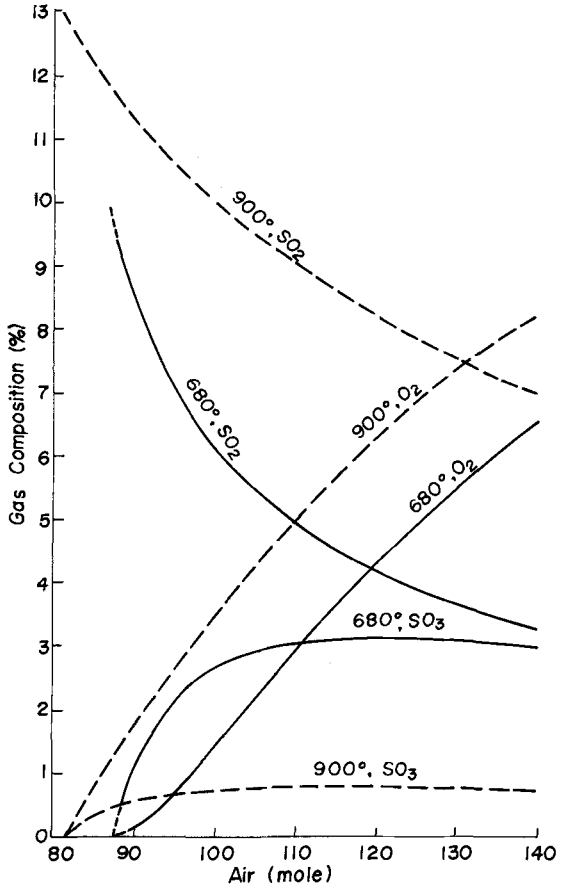

Fig. 8—Equilibrium compositions of roaster gas with varying amount of air per 1 kg concentrate shown in Table I. Solid line: 680°C, dashed line: 900°C.

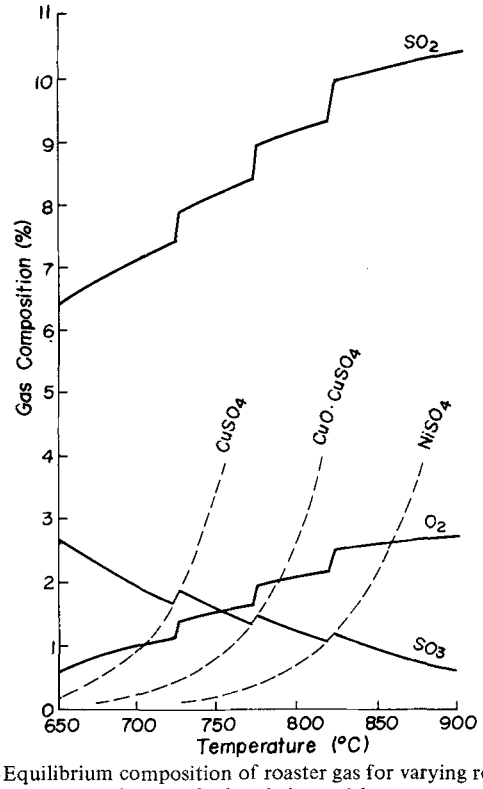

Fig. 9—Equilibrium composition of roaster gas for varying roasting temperature under the use of 96 mol air per 1 kg concentrate.

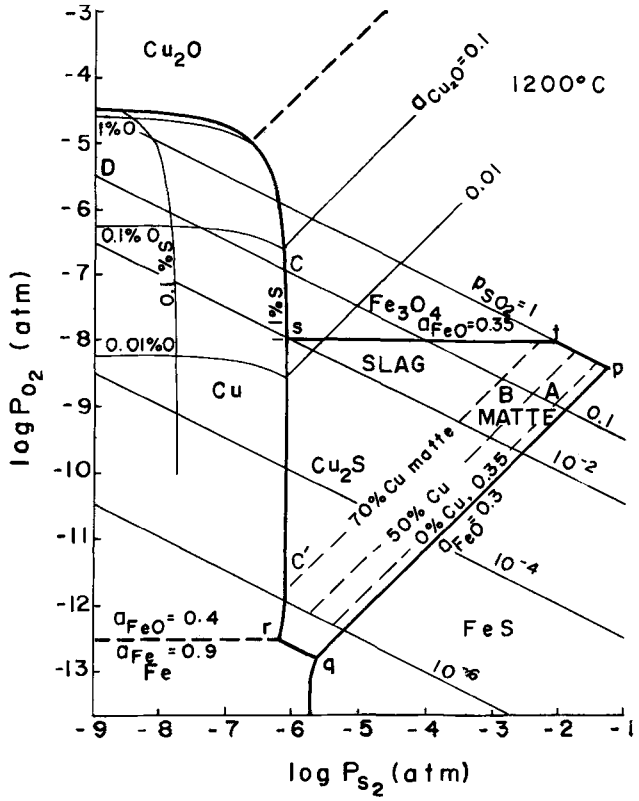

Fig. 10—Sulfur-oxygen potential diagram for Cu-Fe-S-O-SiO_2 system at 1200°C.

The results of these stoichiometric calculations for 680°C are presented in Fig. 8 in which the roaster gas composition is plotted against the amount of air introduced, m. The dashed lines are the results at 900°C assuming a dead roast of the concentrate. It should be noted that increasing the value of m results in a sharp decrease in the SO_2 content, especially in sulfation roasting at 680°C.

Variations in gas composition with temperature are plotted in Fig. 9. The quantity of air introduced is 96 mol which corresponds to an excess of 10 pct over the theoritical amount required for selective sulfation. Decomposition SO_3 pressures of the various sulfates are also included. Similar figures are already presented by Kellogg[19] and hence, precise explanations are not given here.

SMELTING PROCESSES

If the Cu-Fe-S-O system shown in Fig. 6 is considered at smelting temperatures under the coexistence of silica, liquid matte, and slag phases are present and increase the difficulty in the construction of the diagram. The sulfur-oxygen potential diagram for 1200°C is constructed by combining phase equilibria and activity relationships with thermodynamic data and is reproduced in Fig. 10. A detailed explanation of this diagram was given elsewhere[20] and was found to be very useful in explaining both new and conventional copper smelting processes. The lack of reliable data for activity or phase equilibria was clearly recognized during the construction of this type of diagram.

In this figure, liquid matte and slag in equilibrium with a gas phase are represented by the region pqrstp.

The line pq corresponds to a silica saturated slag in equilibrium with an FeS-FeO matte in the absence of copper. By increasing the FeO activity or copper content in the system, line pq shifts towards the upper left as shown by the constant matte grade lines. The line qr represents matte and slag in equilibrium with both silica and γ-iron and corresponds to an extreme case of matte smelting under reducing conditions or a slag cleaning process. The line rs describes the conversion of copper sulfide into liquid copper under the possible coexistence of slag. The upper limit, st, corresponds to the formation of magnetite in a slag in which the FeO activity is 0.35. Finally, under ambient pressure conditions line tp is the boundary for the coexistence of matte and slag.

Commercial oxidation smelting follows the path ABC in Fig. 10. The matte smelting stage is carried out in the region AB under an oxygen pressure of 10^{-8} to 10^{-9} atm at 1200°C with a small variation in oxygen potential with increasing matte grade. Correspondingly, the activities of Fe_3C_4 and Cu_2O vary slightly and suggest that white metal with approximately 75 pct Cu may be produced without serious solid magnetite separation. In contrast, the conversion of Cu_2S to Cu at point C requires an oxygen pressure one hundred times higher resulting in the formation of solid magnetite. Thus, during the finishing stage of converting, a small amount of solid magnetite coexists with white metal and/or crude copper after slag tapping. The significance of the drastic variation in the oxygen potential and Fe_3O_4 and Cu_2O activities during the oxidation of white metal to copper was emphasized[20,21] in connection with the evaluation of new processes and the behavior of minor elements. It should be noted that a decrease in the FeO activity results in an upward shift of the line st which in turn reduces the likelihood of magnetite precipitation. One way to avoid solid magnetite separation is found in the use of a calcium ferrite slag.[22] Moreover, higher temperatures will also suppress magnetite separation. A similar potential diagram for 1300°C suggests that the conversion of Cu_2S to Cu can be realized at an SO_2 partial pressure of 0.1 atm without the formation of solid magnetite. Theoretically, with the application of vacuum during the blister making stage, a coexisting slag may not be hampered by solid magnetite separation or high copper content even at 1200°C.

In Fig. 10, it is seen that metallic copper can be produced directly from Cu_2S by oxidation at point C, corresponding to the converting process, but not through copper oxide. The production of lead metal directly from PbS seems to be quite similar to the case of copper, according to Fig. 3. The possibility of this process was discussed from a thermodynamic standpoint by Schumann *et al*[23] and reviewed by Matyas *et al*[24] citing various practical proposals. The present author also discussed this possibility by utilizing the sulfur-oxygen potential diagram.[25] A recalculated version for 1200°C is presented in Fig. 11, and the conventional lead smelting process may be expressed in this figure by "Oxidation" followed by "Reduction", but a simple oxidation with air or oxygen results in the gradual conversion of PbS into Pb as shown by the region labelled "Direct", where the sulfur content in bullion is 0.5 pct or so.

It is very interesting to compare the merits and

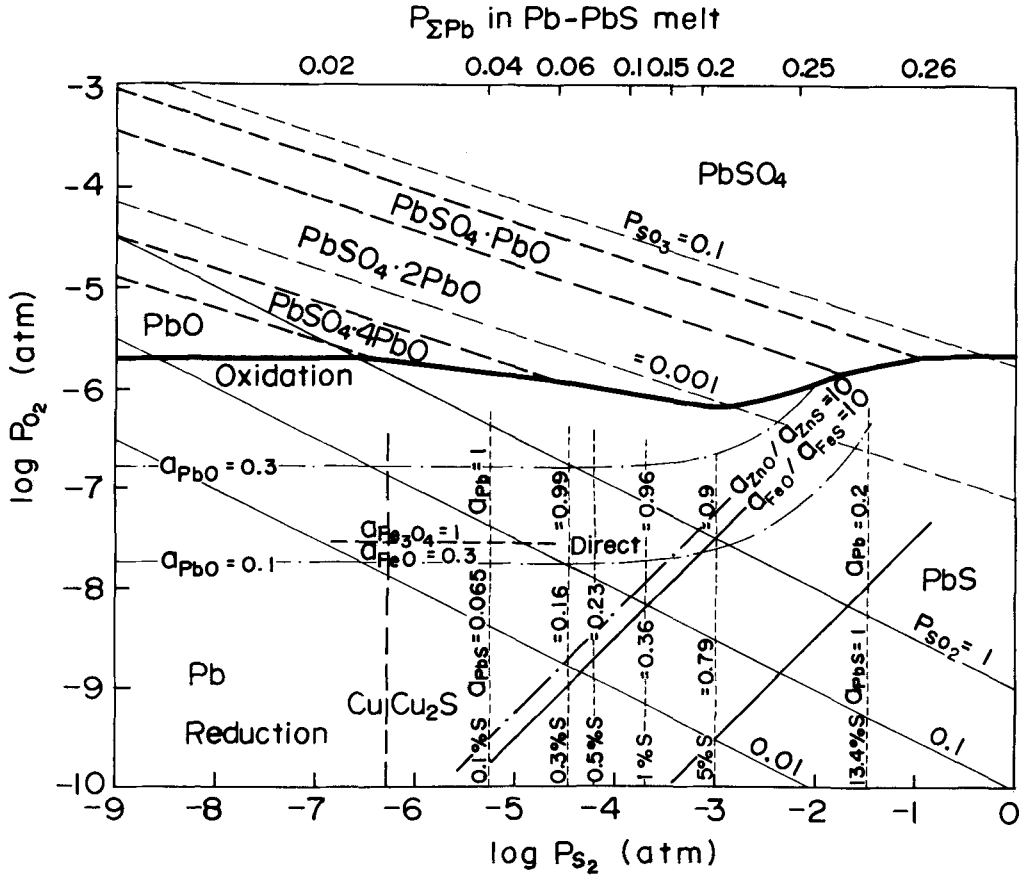

Fig. 11—Sulfur-oxygen potential diagram for Pb-S-O system at 1200°C to explain lead smelting.

demerits of direct lead production with that of copper. As suggested by Fig. 3, the stability of lead metal is not inferior to that of copper along the 0.1 atm SO_2 isobar. In fact, the oxygen potential required for PbS conversion is much lower, suggesting that the difficulties associated with magnetite formation may be reduced. Moreover, the thermodynamic behavior of some impurities such as arsenic and antimony which must be carefully taken into account in direct copper production is not as significant in the case of lead. An additional practical merit in direct lead smelting is that the amount of slag is greatly reduced because the content of gangue is considerably lower in lead concentrate.

Demerits of the process are found in a detailed examination of the potential diagrams. Conversion of Cu_2S into copper takes place at point C in Fig. 10 or point e in Fig. 3 where both the activities of Cu_2S and Cu are nearly unity. However, due to the single eutectic type Pb-PbS system, the conversion of PbS takes place gradually; and thus, an equal activity point between Pb and PbS, such as point c in Fig. 3, is too low in oxygen potential to obtain desulfurized liquid lead. This situation is clearly illustrated in Fig. 11 which shows that in order to obtain lead bullion containing 0.3 to 0.5 pct sulfur, an activity of PbO of 0.1 to 0.2 is inevitable at 1200°C. In conjunction, the activity coefficient of $CuO_{0.5}$ is approximately 3 in fayalite type slags while that of PbO may be less than unity. Therefore, a higher metal content in slag is unavoidable for the direct smelting of lead. Furthermore, as pointed out in connection with roast reaction processes, the high vapor pressure of lead compounds and the high melting point of zinc compounds may lead to problems in direct smelting.

In Fig. 11, additional informations on other elements are also shown to better understand direct lead smelting. To obtain lead bullion containing 0.3 to 0.5 pct S by use of air or oxygen, the activity of FeO must be maintained at low levels to avoid the formation of solid magnetite, as indicated in the figure. According to the oxide-sulfide activity ratio lines, zinc and iron sulfides in the concentrate may be expected to be satisfactorily oxidized. In reference to Fig. 10, it is estimated that considerable amounts of copper will remain as a sulfide to form a relatively high grade matte phase containing PbS and FeS.

The effective vapor pressure, $p_{\Sigma Pb}$, defined along a given p_{SO_2} isobar as the sum of $p_{PbS} + 2\,p_{Pb_2S_2} + p_{Pb} + p_{PbO} + 2\,p_{Pb_2O_2} + 3\,p_{Pb_3O_3} + 4\,p_{Pb_4O_4}$ is plotted along the upper scale in Fig. 11 and indicates that vaporization loss must be carefully taken into account. Considering that the vapor pressure of pure PbO and pure Pb are of the same order and that the PbO activity is small, the contribution of oxide vapor species is small. Judging from the values of $p_{\Sigma Pb}$ in the figure, equilibrium vapor pressures in direct smelting are a few times higher than in the conventional process.

Summarizing these observations obtained from the potential diagram, an effective direct lead smelting process requires the minimum use of a low melting point, fluid slag with a low FeO activity and a high PbO activity coefficient. In order to decrease vaporization loss, low operation temperature, low sulfur bullion, and use of oxygen will be convenient. Unfortunately, these conditions all tend to increase the activity of PbO. The optimum conditions are discussed in detail, separately.[26]

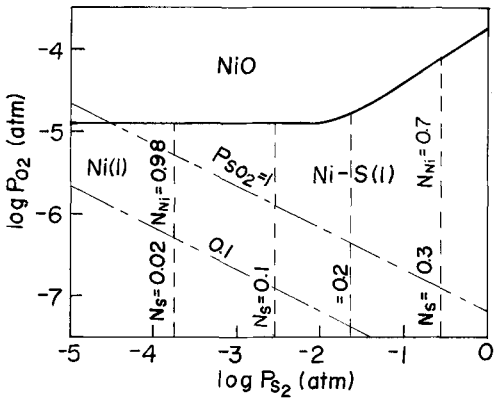

Fig. 12—Sulfur-oxygen potential diagram for Ni-S-O system at 1450°C.

Direct smelting of nickel sulfide into metal appears to be difficult at 1027°C according to Fig. 3 due to the low oxygen and sulfur dioxide pressures involved. However, increasing the temperature results in an increase in the stability of the metal. Figure 12 is the potential diagram for the Ni-S-O system at 1450°C, in which the activity data obtained by Remen *et al*[27] are also used. Judging from the location of the SO_2 isobars, successful direct conversion into metal may be achieved at higher temperatures. This is contrary to the traditional view that the nickel sulfide smelting process must be terminated at the concentrated matte, Ni_3Si_2, stage and that converting to metal can not be realized. In fact, a similar potential diagram at 1250°C suggests the difficulties in producing nickel directly. However, INCO has carried out the direct production of metal from concentrated matte in their TBRC[28] operation, a high temperature, homogeneous oxidation process.

Stoichiometric computer calculations were successfully performed by Goto[29] and Nagamori *et al*[30] mainly for copper smelting. Although not discussed here, these results again reinforce the use of thermodynamic calculations for the evalaution of metallurgical processes.

RECOVERY OF SULFUR IN THE OXIDATION PROCESS

Although in most sulfide smelters, the exhaust gas is converted to sulfuric acid, elemental sulfur is sometimes preferred depending on the market. However, reduction of SO_2 by consuming fossil fuels is too expensive and the search is on for a new process to economically produce both elemental metal and sulfur. Undoubtedly, hydrometallurgy offers one hopeful route but the convenience of recovering elemental sulfur pyrometallurgically during oxidation cannot be ignored. Judging from Fig. 3, recovery of sulfur from iron sulfide during oxidation is the most favorable because the conversion of FeS to Fe_3O_4 at point a in Fig. 3 represents the highest sulfur pressure. In addition, if the starting material is FeS_2, one sulfur atom is obtained simply by dissociation, as shown in Fig. 5. However, judging from the proportions of SO_2 and S_2, if the gas at point a in Fig. 3 is cooled directly, the recovery of sulfur will be at most a few percent. The relation be-

tween SO_2 and S_2 is defined thermodynamically and high sulfur recovery is doubtful when FeS is oxidized by air in the normal manner.

If the nitrogen in air is substituted with water vapor and this H_2O-O_2 gas mixture is used for the oxidation, quantities of H_2 and H_2S are formed as suggested by the H_2O/H_2 and H_2S/H_2 scales in Fig. 3. When the product gas containing SO_2, S_2, H_2, H_2S, and H_2O is cooled to a temperature convenient for the Claus reaction to proceed, a considerable recovery of elemental sulfur is expected.

The treatment of sulfide ores with H_2O-O_2 gas mixtures was proposed by Norman[31] but lacked quantitative data and clarification of the optimum conditions.

Stoichiometric calculations incorporating thermodynamic data provide the necessary information to determine the optimum conditions for sulfur recovery. In the following example, an excess amount of solid FeS is oxidized to Fe_3O_4 by a gas consisting of 70 mol of H_2O and 30 mol of oxygen at 1 atm.

Reactants: FeS(in excess), 70 mol of H_2O, 30 mol of O_2

Products: Fe_3O_4, S_2, SO_2, H_2, H_2S, H_2O, (SO),

Fe balance: $$n_{FeS} = 3\, n_{Fe_3O_4} \quad [35]$$

S balance: $$n_{FeS} = 2\, n_{S_2} + n_{SO_2} + n_{H_2S} \quad [36]$$

O balance: $$70 + 2 \times 30 = 4\, n_{Fe_3O_4} + 2\, n_{SO_2} + n_{H_2O} \quad [37]$$

H balance: $$2 \times 70 = 2\, n_{H_2S} + 2\, n_{H_2O} + 2\, n_{H_2} \quad [38]$$

where n denotes number of moles, n_{FeS} is the number of moles of FeS reacted, and n_{H_2O} is the number of moles of H_2O in the product gas. The total mole number of the gaseous phase is,

$$n_T = n_{SO_2} + n_{H_2} + n_{S_2} + n_{H_2S} + n_{H_2O} \quad [39]$$

Using available free energy data, the following equations are also derived:

$$1/2\ S_2 + O_2 = SO_2 \quad K_{40} = (n_{SO_2} \cdot n_T^{1/2})/(n_{O_2} \cdot n_{S_2}^{1/2}) \quad [40]$$

$$H_2 + 1/2\ O_2 = H_2O \quad K_{41} = (n_{H_2O} \cdot n_T^{1/2})/(n_{H_2} \cdot n_{O_2}^{1/2}) \quad [41]$$

$$H_2 + 1/2\ S_2 = H_2S \quad K_{42} = (n_{H_2S} \cdot n_T^{1/2})/(n_{H_2} \cdot n_{S_2}^{1/2}) \quad [42]$$

$$6\ FeS + 4\ O_2 = 2\ Fe_3O_4 + 3\ S_2 \quad K_{43} = n_{S_2}^3 \cdot n_T / n_{O_2}^4 \quad [43]$$

Solutions for the nine unknowns, n_{SO_2}, n_{H_2}, n_{S_2}, n_{H_2S}, n_{H_2O}, n_{O_2}, n_T, n_{FeS}, and $n_{Fe_3O_4}$ can be derived by solving the above nine equations.

Repeating similar stoichiometric calculations, variations in equilibrium gas compositions as a function of temperature are generated and illustrated in Fig. 13 for initial H_2O:O_2 mole ratios of 80:20 and 70:30. The appearance of a liquid phase at the higher temperatures is neglected and the activities of FeS and Fe_3O_4 are always assumed to be unity. According to Fig. 13, the variations in H_2O, SO_2, and H_2S pressures for a given initial gas ratio are small but decrease slightly with increasing temperature. To compensate, the H_2 and S_2 pressures increase as temperature increases.

The product gas composition corresponding to an initial H_2O:O_2 mold ratio of 80:20 is submitted to an

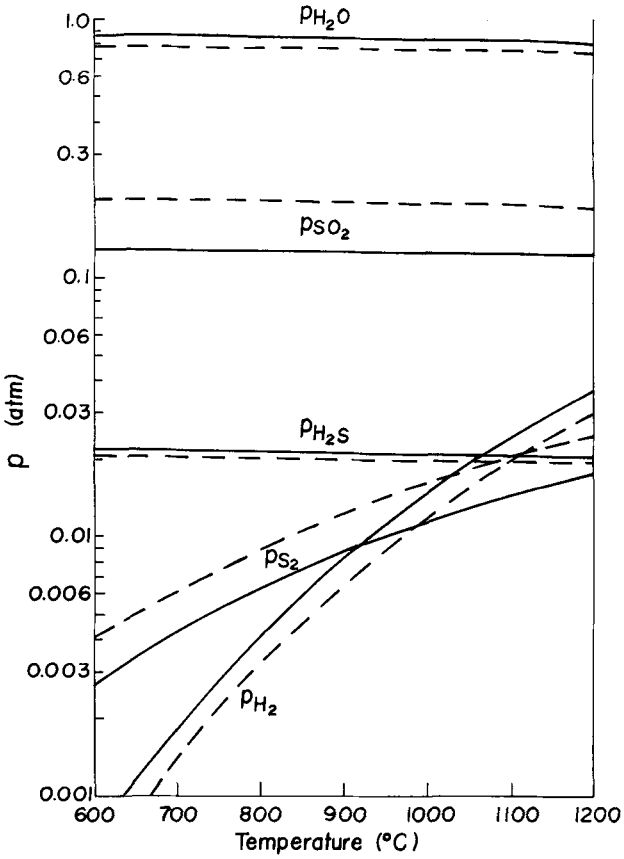

Fig. 13—Composition of gas obtained from the reaction between FeS and H_2O-O_2 gas at varying oxidation temperature. Initial H_2O to O_2 ratio is, 80 : 20 solid lines
70 : 30 dashed lines.

equilibrium Claus reaction calculation for 200°C in the absence of FeS and Fe_3O_4. The calculations are performed using similar techniques to those described above and the results are illustrated in Fig. 14. At 200°C, S_8 is the predominant gas species for sulfur while the partial pressure of S_2 is only 10^{-6} atm. Almost all the H_2 and H_2S react with SO_2 to produce sulfur gas, but is should be noted that approximately 0.15 pct H_2S remains along with a considerable amount of SO_2.

In Fig. 14, the mole number of reacted FeS is also given and increases with increasing temperature. The recovery of elemental sulfur is defined on the basis of this reacted quantity of FeS as follows:

$$R_S = \frac{2\, n_{S_2} + 6\, n_{S_6} + 8\, n_{S_8}}{n_{FeS}} \times 100 \text{ pct} \quad [44]$$

The value of R_S is also included in Fig. 14 suggesting that the recovery increases considerably with increasing temperature.

Various other possibllities are treated including the incorporation of a liquid phase in the system.[32] It is worthwhile to consider the application of this process to copper smelting in which the principal reaction is the oxidation of FeS to FeO. Also, as suggested in Fig. 10, the variation of the sulfur potential is relatively small during the matte smelting stage. One requirement is the availability of an effective recycle system for steam.

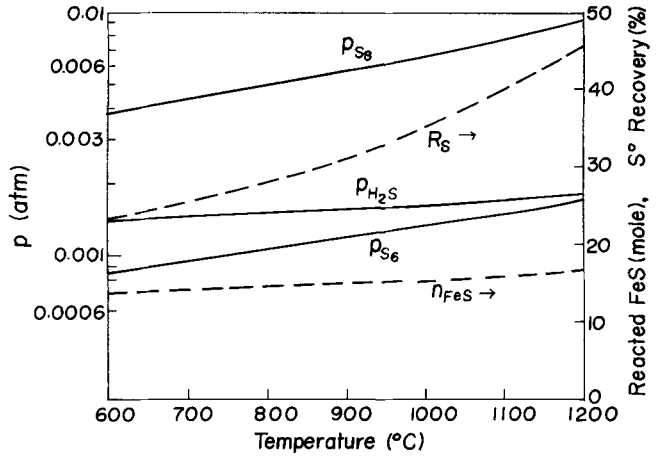

Fig. 14—Influence of the preceding oxidation temperature on the possible recovery of sulfur after Claus reaction at 200°C. Solid lines: equilibrium gas composition at 200°C. R_s : recovery of elemental sulfur gas. η_{FeS} : amount of reacted FeS in the preceding oxidation.

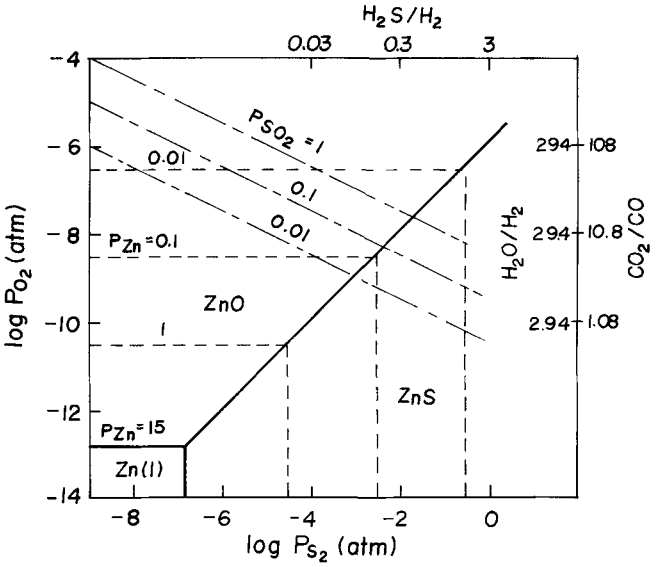

Fig. 15—Sulfur-oxygen potential diagram for Zn-S-O system at 1270°C with special interest in direct distillation of ZnS.

VAPORIZATION OF ZINC DURING OXIDATION OF SULFIDE

It is suggested in Fig. 3 that the direct oxidation of zinc sulfide to metal is hardly possible at 1027°C. Figure 15 shows a similar diagram at 1270°C and reveals a considerable increase in the vapor pressure of zinc. If the oxidation of ZnS by air is considered along the 0.1 atm SO_2 isobar at 1270°C, the maximum zinc pressure occurs when ZnS and ZnO coexist and reaches nearly 0.1 atm. Therefore, it may be concluded that when ZnS converts to ZnO, the volatility of zinc becomes a maximum and a considerable amount of zinc vapor is stable at the smelting temperature. It has already been pointed out[33] that the "oxidation-volatilization" phenomenon may be the principal mechanism for the volatilization of zinc during copper smelting.

Figure 15 raises the possibility of the direct distillation of zinc sulfide by a simple oxidation process excluding a reducing step. The potential diagrams indicate that a higher temperature and lower SO_2 pressure improve the recovery of zinc metal gas, but decreasing the temperature easily results in the reoxidation or resulfidation of the zinc vapor. Moreover, differing from the conventional roasting of zinc sulfide, the formation of zinc vapor by the oxidation of ZnS is not thermally favorable and considerable heat compensation may be required.

A schematic flowsheet is illustrated in Fig. 16 for the direct distillation of zinc sulfide. To simplify the conditions, 100 mol of air containing 20.6 pct oxygen are preheated to the required temperature and then reacted with oil to consume 12.6 mol of oxygen. The exiting combustion gas containing 8 mol of oxygen is introduced into the reaction zone where the oxidation of ZnS takes place to produce metallic zinc vapor. The resultant gas containing approximately 8 pct zinc enters a condenser to collect the zinc as a liquid phase. The exhaust gas from the condenser containing around 8 pct SO_2 is sent to the acid plant.

Given the air composition shown in Table II, 12.6 mol of oxygen react with oil having a composition of 85.1 pct C and 11.8 pct H. Thus, the combustion gas with the composition shown in Table II will be obtained by consuming 125.5 g of oil. Assuming that the 103.7 mol of combustion gas react completely with excess ZnS, the reaction products are evaluated quantitatively by using stoichiometric calculations along with thermodynamic data. The essential components are as follows:

Reactants: ZnS, O_2, CO_2, H_2O
Products: ZnO, Zn, S_2, SO_2, SO, CO, CO_2, H_2, H_2O, COS, H_2S

N_2 and excess ZnS remain with the products. The mole balances between the reactants and products are as follows:

$$\text{Zn: } n_{ZnS} = n_{ZnO} + n_{Zn} \quad [45]$$

$$\text{S: } n_{ZnS} = 2n_{S_2} + n_{SO_2} + n_{SO} + n_{COS} + n_{H_2S} \quad [46]$$

$$\text{O: } 16 + 17.8 + 9.1 = n_{ZnO} + 2n_{SO_2} + n_{SO} + n_{CO} + 2n_{CO_2} + n_{H_2O} + n_{COS} \quad [47]$$

$$\text{C: } 8.9 = n_{CO} + n_{CO_2} + n_{COS} \quad [48]$$

$$H_2\text{: } 9.1 = n_{H_2} + n_{H_2O} + n_{H_2S} \quad [49]$$

n is the number of moles of each product while n_{ZnS} is the participating number of moles of ZnS in the reaction. The total number of moles of the gaseous species is,

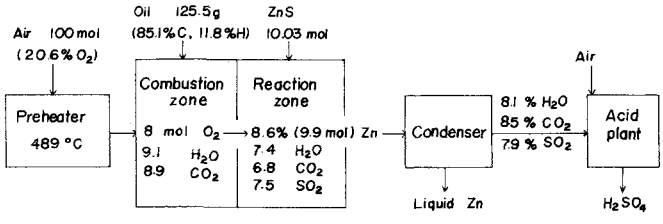

Fig. 16—Schematic flowsheet of direct distillation process of ZnS.

Table II. Composition of Gases in Various Stages in Direct Extraction of Zinc

	Air, Mol	Combustion gas, Mol	Gas reacted with ZnS at 1270°C		Gas after condensation of zinc at 500°C	
			Mol	Pct	Mol	Pct
N_2	77.7	77.7	77.7	67.5	77.7	74.3
O_2	20.6	8.0	$4.8.10^{-7}$		$2.6.10^{-19}$	
H_2O	1.7	9.1	8.56	7.44	8.43	8.06
CO_2		8.9	7.78	6.76	8.89	8.51
SO_2			8.59	7.47	8.29	7.93
S_2			0.49	0.43	0.53	0.51
SO			0.36	0.31	$1.1.10^{-4}$	
CO			1.11	0.96	$4.9.10^{-4}$	
COS			0.01	0.01	$8.3.10^{-3}$	0.01
H_2			0.45	0.39	$2.8.10^{-3}$	
H_2S			0.09	0.08	0.67	0.64
Zn			9.92	8.62		
Total	100	103.7	115.06	100	104.52	100
ZnS reacted			10.03			

$$n_T = 77.7 + n_{Zn} + n_{S_2} + n_{SO_2} + n_{SO} + n_{CO} + n_{CO_2} + n_{COS} + n_{H_2} + n_{H_2O} + n_{H_2S} \quad [50]$$

Under 1 atm, the relevant equilibrium relations are,

$$1/2\,S_2 + O_2 = SO_2 \quad K_{51} = (n_{SO_2} \cdot n_T^{1/2})/(n_{O_2} \cdot n_{S_2}^{1/2}) \quad [51]$$

$$1/2\,S_2 + 1/2\,O_2 = SO, \quad K_{52} = n_{SO}/(n_{S_2}^{1/2} \cdot n_{O_2}^{1/2}) \quad [52]$$

$$2\,ZnO(s) = 2\,Zn(g) + O_2, \quad K_{53} = n_{Zn}^2 \cdot n_{O_2}/n_T^3 \quad [53]$$

$$2\,ZnS(s) = 2\,Zn(g) + S_2, \quad K_{54} = n_{Zn}^2 \cdot n_{S_2}/n_T^3 \quad [54]$$

$$CO + 1/2\,O_2 = CO_2, \quad K_{55} = (n_{CO_2} \cdot n_T^{1/2})/(n_{CO} \cdot n_{O_2}^{1/2}) \quad [55]$$

$$H_2 + 1/2\,O_2 = H_2O, \quad K_{56} = (n_{H_2O} \cdot n_T^{1/2})/(n_{H_2} \cdot n_{O_2}^{1/2}) \quad [56]$$

$$CO + 1/2\,S_2 = COS, \quad K_{57} = (n_{COS} \cdot n_T^{1/2})/(n_{CO} \cdot n_{S_2}^{1/2}) \quad [57]$$

$$H_2 + 1/2\,S_2 = H_2S, \quad K_{58} = (n_{H_2S} \cdot n_T^{1/2})/(n_{H_2} \cdot n_{S_2}^{1/2}) \quad [58]$$

Fourteen unknown quantities are solved from these fourteen simultaneous equations.

The calculated results at 1270°C are presented in Table II in both percent and mole number. Oxygen is consumed completely and a gas containing 8.62 pct of metallic zinc vapor is produced from 10.03 mol of ZnS. The recovery of zinc vapor is approximately 99 pct but this zinc vapor tends to convert to ZnS and ZnO during cooling because considerable amounts of CO_2, SO_2, and H_2O are also present in the gas. Therefore, the gas must be quenched in a specially designed condenser to recover zinc as liquid metal.

Solving the fourteen equations is not an easy task even with the aid of a computer and it should be emphasized that the approximate results are estimated at a glance from Fig. 15 which can be constructed quite easily. Of course, the detailed numerical quantities must be generated through complex mathematical procedures. However, to obtain the basic concepts for new processes and to perform a semiquantative evaluation of metallurgical operations, the chemical potential diagram is certainly a useful tool.

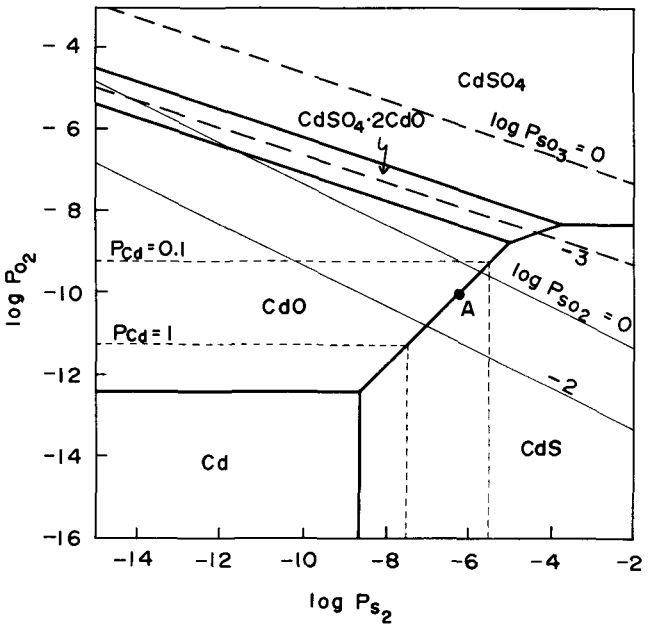

Fig. 17—Sulfur-oxygen potential diagram for Cd-S-O system at 900°C.

Returning to Table II, the equilibrium gas composition at 500°C following the condensation of zinc vapor is derived by similar calculation methods and tabulated. This exhaust gas is suitable not only for the usual acid plant but also for a Claus reactor with additions of H_2S to recover sulfur in elemental form.

This direct distillation process is also interesting from a required energy perspective. Several engineering hurdles such as condenser design and the separation of dust from the complex gas are predicted.[34] However, a detailed discussion of these areas is beyond the scope of this paper.

A similar phenomenon of oxidation-volatilization can be observed in the oxidation of cadmium sulfide as illustrated in Fig. 17. Because cadmium is more noble and possesses a higher vapor pressure than zinc, cadmium sulfide is not converted directly to the oxide form during the roasting of zinc concentrate but volatilizes at first as cadmium metal which then may

be oxidized or sulfatized by the excess oxygen in the bulk roaster gas.[35]

An extreme case of oxidation-volatilization occurs with mercury which is not easily converted into oxide or sulfate after vaporization. This is very convenient for mercury production which requires a simple condensation process to recover liquid mercury. However, the difficulty in sulfatizing mercury is inconvenient for the roasting and smelting of sulfide concentrates as it is difficult to precipitate mercury with conventional gas cleaning systems. Thus, a small fraction of mercury sometimes reaches the acid plant, and special removal methods are required.[36]

SEGREGATION PROCESS FOR COPPER OR NICKEL OXIDE ORES

Many researchers have been interested in the segregation process for the extraction of copper or nickel from low grade oxide ores. At present, considerable discrepancies are observed concerning the adaptability of these processes to practice. This confusion is ascribed to the fact that the segregation reactions are so complex that an exact understanding of the optimum conditions is difficult. Many efforts have been made to clarify the mechanism and the optimum conditions. From a thermodynamic standpoint, Iwasaki[37] published an interesting report making use of the oxygen-chlorine chemical potential diagram.

Although various detailed opinions have been presented hitherto, the following three reactions are generally accepted as the principla mechanism for the copper segregation process:

$$2\,NaCl(l) + SiO_2(s) + H_2O(g) = Na_2SiO_3(s) + 2HCl(g) \quad [59]$$

$$Cu_2O(s) + 2\,HCl(g) = 2/3\,Cu_3Cl_3(g) + H_2O(g) \quad [60]$$

$$2/3\,Cu_3Cl_3(g) + H_2(g) = 2\,Cu(s) + 2\,HCl(g) \quad [61]$$

In a mixture consisting of ore, salt, and carbon, these quite different reactions must take place at adjacent sites. The reaction represented by Eq. [61] must occur under the strong reducing conditions found near the surface of carbon. The product HCl gas must be transported to a higher oxygen potential site to produce Cu_3Cl_3 gas in accordance with Eq. [60]. Finally, the released H_2O of Eq. [60] must return as the reactant in Eq. [59].

Assuming that local equilibria are established in each step at each site, a thermodynamic evaluation can be performed. From the localized concentrations thus generated for the various gaseous species, one can evaluate the feasibility of this process.

As the basis for this calculation, 100 g of feed pellets having the composition shown in Table III are considered. The amounts of chlorides and carbon are varied depending on the conditions and some H_2O is also essential. As a result of the segregation reactions, a considerable amount of gas is evolved and gradually flows outward from the pellet. Therefore, it is considered that the segregation equilibria are established inside the pellet without appreciable influence from the bulk furnace gas.

As an example of the equilibrium evaluation of the copper segregation process, 100 g of pellets described in Table III are held at 827°C along with 1.14 g (0.0633 mol) of H_2O. 0.9 g (0.0154 mol) of NaCl convert into HCl consuming 0.14 g (0.0077 mol) of H_2O. 0.3 g (0.025 mol) of C react and produce CO and CO_2 gases. From the following stoichiometric and thermodynamic relations, the local gas compositions in equilibrium with each respective solid phase are evaluated at ambient pressure based upon free energy data:[38]

$$\text{C balance: } 0.0250 = n_{CO} + n_{CO_2} \quad [62]$$

$$H_2 \text{ balance: } 0.0633 = n_{H_2O} + n_{H_2} + 1/2\,n_{HCl} \quad [63]$$

$$\text{Cl balance: } 0.0154 = n_{HCl} + 2\,n_{FeCl_2} + 3\,n_{Cu_3Cl_3} + n_{CuCl} \quad [64]$$

$$n_T = n_{H_2O} + n_{H_2} + n_{CO_2} + n_{CO} + n_{Cu_3Cl_3} + n_{CuCl} + n_{HCl} + n_{FeCl_2} \quad [65]$$

$$Cu_2O(s) + 2\,HCl(g) = 2/3\,Cu_3Cl_3(g) + H_2O(g) \quad [60]$$

$$K_{60} = n_{Cu_3Cl_3}^{2/3} \cdot n_{H_2O} \cdot n_T^{1/3} / n_{HCl}^2$$

$$2/3\,Cu_3Cl_3(g) + H_2(g) = 2\,Cu(s) + 2\,HCl(g) \quad [61]$$

$$K_{61} = n_{HCl}^2 / n_{Cu_3Cl_3}^{2/3} \cdot n_{H_2} \cdot n_T^{1/3})$$

$$Fe_2O_3(s) + 4\,HCl(g) + H_2(g) = 2\,FeCl_2(g) + 3\,H_2O(g) \quad [66]$$

$$K_{66} = (n_{FeCl_2}^2 \cdot n_{H_2O}^3) / (n_{HCl}^4 \cdot n_{H_2})$$

$$Fe_3O_4(s) + 6\,HCl(g) + H_2(g) = 3\,FeCl_2(g) + 4\,H_2O(g) \quad [67]$$

$$K_{67} = (n_{FeCl_2}^3 \cdot n_{H_2O}^4) / (n_{HCl}^6 \cdot n_{H_2})$$

$$1/2\,Fe_2SiO_4(s) + 2\,HCl(g) = FeCl_2(g) + 1/2\,SiO_2(s) + H_2O(g) \quad [68]$$

$$K_{68} = (n_{FeCl_2} \cdot n_{H_2O}) / n_{HCl}^2$$

$$CO(g) + H_2O(g) = CO_2(g) + H_2(g) \quad [69]$$

$$K_{69} = (n_{CO_2} \cdot n_{H_2}) / (n_{CO} \cdot n_{H_2O})$$

$$3\,CuCl(g) = Cu_3Cl_3(g) \quad [70]$$

$$K_{70} = n_{Cu_3Cl_3} \cdot n_T^2 / n_{CuCl}^3$$

The results for 827°C are presented in Fig. 18 in which the partial pressures are plotted against oxygen potential. The presence of stable solid phases depends on

Table III. Composition of Pellets for Segregation Reaction

Copper pellet		Nickel pellet	
Constituents	Content Pct	Constituents	Amount, g
Cu	2	Ni	2
Fe	20	Fe	20
NaCl	1	$CaCl_2$	6
C	1	C	3
gangue	balance	gangue	balance

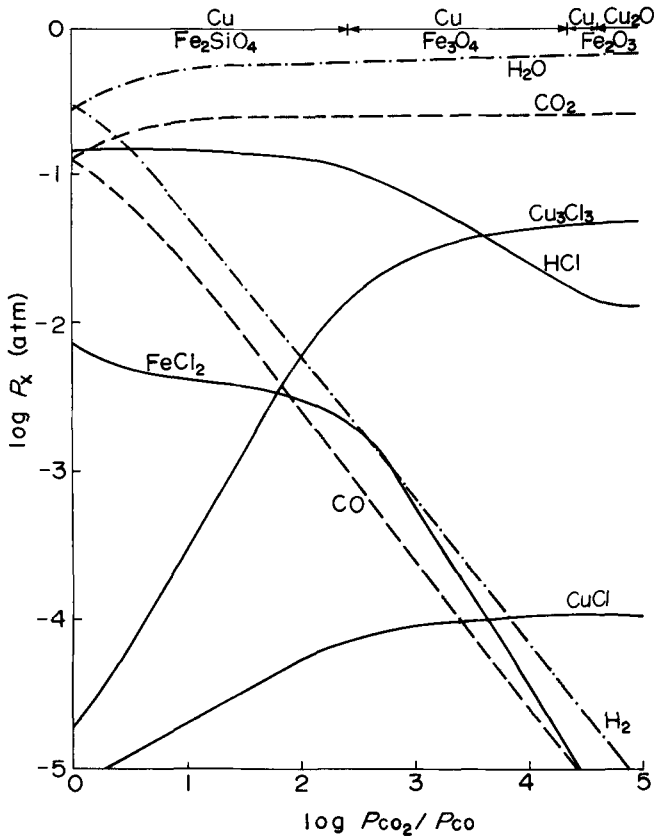

Fig. 18—Resulting partial pressures in copper segregation system plotted against oxygen potential at 827°C. Amounts participating in the reaction are as follows:
C : 0.3 Pct, NaCl : 0.9 Pct, H_2O : 1.14 Pct

the oxygen potential and are located at the top of the figure. The activities of these condensed species are always taken as unity.

As shown in Fig. 18, the evolved gas consists mainly of Co_2 and H_2O in accordance with practical observations.[39] The equilibrium pressure of Cu_3Cl_3 is considerable in the region where copper oxide is stable suggesting that the chlorination reaction of Eq. [60] proceeds satisfactorily. Also, the Cu_3Cl_3 pressure decreases sharply with decreasing oxygen potential because Eq. [61] occurs to produce metallic copper. In the reverse direction, HCl produced at low oxygen potential via Eq. [61] will be transported to the higher oxygen potential region and consumed in the reaction represented by Eq. [60]. Thus, the sharp gradients in the partial pressures of Cu_3Cl_3 and HCl are ideal for the segregation reactions. Cu_3Cl_3 is drawn to and reduced on the carbon surface and the produced HCl is transported back to the region where Cu_2O exists and is recycled within the pellet for chlorination. The contribution of $FeCl_2$ is relatively small or negilgible especially in the higher oxygen potential region when compared with HCl.

Detailed calculations[40] suggest that from a thermodynamic standpoint, decreasing the temperature, decreasing the amount of H_2O and increasing the amount of NaCl will enhance the copper segregation reactions. Because excess H_2O simply consumes NaCl, the quantity of water should be maintained at minute levels.

Similar calculations are possible for nickel segregation equilibria and the results are illustrated in Fig. 19. The participating amounts of C, $CaCl_2$, and H_2O are 1, 2, and 0.37 g respectively for a 100 g pellet. Because of the relative instability of $NiCl_2$ in comparison with Cu_3Cl_3, the amount of participating H_2O is considered to be extremely small. Taking into account the activity relationship for the Ni-Fe solid solution, the compositions of ferro-nickel alloys are included on the upper scale of Fig. 19.

A sharp decrease in vapor pressure is observed for $NiCl_2$, similar to Cu_3Cl_3, which indicates that the transportation of $NiCl_2$ gas to the carbon surface is possible. However, unlike the previous case, considerably high vapor pressures of HCl and $FeCl_2$ are observed in Fig. 19 and that of HCl does not decrease at the higher oxygen potential region. Therefore, the chloride vapors will tend to escape from the pellet into the bulk furnace gas and recycle of HCl within the pellet cannot be expected. This emission of chlorides was reported by Rey[41] in the case of nickel segregation. Accordingly, a higher consumption of chloridizing agent is inevitable in nickel segregation.

Similar calculations[40] reveal that the $NiCl_2$ partial pressure increases with increasing temperature, increasing $CaCl_2$ amount, and decreasing amount of participating carbon. The effect of H_2O is serious and increasing its quantity results in a sharp decrease in the $NiCl_2$ partial pressure. Thus, complete dehydration is particularly important for nickel segregation.

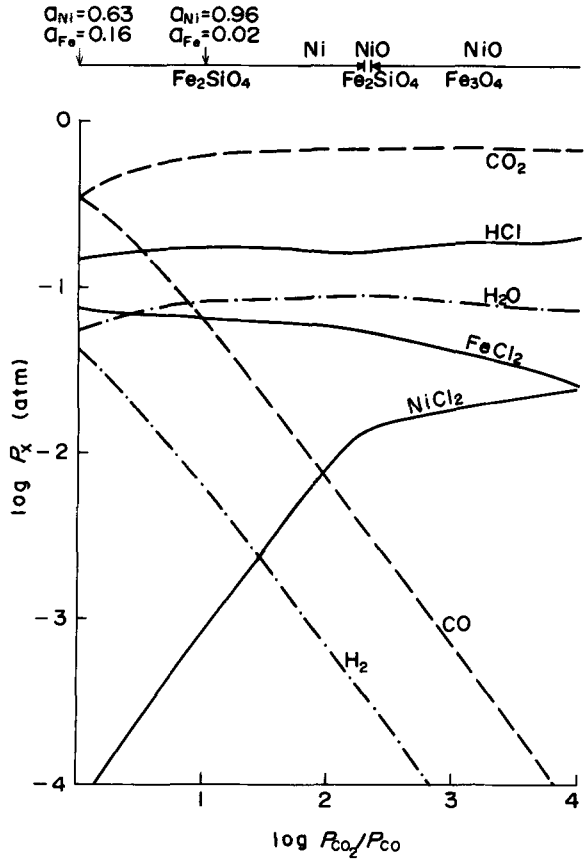

Fig. 19—Resulting partial pressures in nickel segregation system plotted against oxygen potential at 927°C. Amounts participating in the reaction are as follows:
C : 1 Pct, $CaCl_2$: 2 Pct, H_2O : 0.37 Pct

The gradients in the chloride vapor pressures with decreasing oxygen potential are similar but somewhat sharper for Cu_3Cl_3 than $NiCl_2$. Considering that copper chloride is a trimer and begins to be reduced at a higher oxygen potential than nickel chloride, the separation of copper is much easier than that of nickel.

Summarizing these observations, the fundamental reaction calculations are promising for the copper segregation process. However, various serious restrictions are present in nickel segregation. Therefore, efforts should be directed towards successfully developing the copper segregation process prior to tackling the case for nickel.

CONCLUDING REMARKS

Material resources, environmental restrictions, labor policy, and the energy crisis have placed nonferrous extractive metallurgy in a revolutionary period calling for the development of nonpolluting, high efficiency, new processes. In this broad and complex field, there exists an unlimited number of possible studies leading to novel processes. Although we may use various tools to foster new inroads, a thermodynamic approach is undoubtedly the most fundamental. After determining possible routes using chemical potential diagrams, the optimum conditions can be quantitatively evaluated by stoichiometric calculations combined with thermodynamic data. The examples cited in this paper are not readily amenable to practice but similar techniques will certainly aid the young researchers and engineers who will be developing the metallurgy of the future.

ACKNOWLEDGMENT

The author wishes to express his sincere gratitude to Professors S. Matoba, K. Ono, and M. Kameda for their long cordial guidance and encouragement. He is indebted to Dr. G. H. Kaiura, University of Toronto, for his aid in preparing this manuscript.

REFERENCES

1. N. Masuko: Denki Kagaku, 38 (1970), 153; 226; 307.
2. A Yazawa and M. Eguchi: *Hydrometallurgy and Waste Water Treatment,* Kyoritsu Publishing Co., 1975.
3. A. S. Russell, J. D. Edwards, and C. S. Taylor: *J. Metals,* 1955, vol. 7, p. 1123.
4. E. Peters: *Met. Trans. B,* 1976, vol. 7B, p. 505.
5. N. Masuko: *Denki Kagaku,* 1959, vol. 27, p. 365.
6. L. G. Sillen: *Stability Constants of Metal-Ion Complexes,* Chemical Society, London, 1971.
7. W. M. Latimer: *Oxidation Potentials,* Prentice Hall, 1952.
8. M. Kameda: *Sci. Rep. Res. Inst. Tohoku Univ. Ser. A,* 1949, vol. 1, p. 223.
9. V. Lund: *Acta Chim. Scand.,* 1951, vol. 5, p. 555.
10. J. P. Coughlin: U. S. Bur. Mines, Bull. no. 542, 1954.
11. F. D. Richardson and J. H. E. Jeffes: *J. Iron Steel Inst.,* vol. 171, p. 165.
12. H. H. Kellogg: *Trans. TMS-AIME,* 1964, vol. 9B, p. 337.
13. T. Rosenqvist: *Met. Trans. B,* 1978, vol. 9B, p. 337.
14. E. G. King, Alla D. Mah, and L. B. Pankratz: *Thermodynamic Properties of Copper and Its Inorganic Compound,* INCRA, 1973.
15. H. H. Kellogg *et al.: Trans. TMS-AIME,* 1960, vol. 281, p. 70; 1963, vol. 227, p. 1419; 1966, vol. 236, p. 602.
16. T. R. Ingraham and R. Kerby: *Can. Metall. Quart.,* 1967, vol. 6, p. 89.
17. H. Kurushima and S. Tsunoda: *J.Metals, 1955,* vol. 7, p. 634.
18. L. F. Theys *et al.: J. Metals,* 1958, vol. 10, pp. 134, 476; vol. 16, p. 831.
19. H. H. Kellogg: *J. Metals,* 1956, vol. 8, p. 1105.
20. A. Yazawa: *Can. Metall. Quart.,* 1974, vol. 13, p. 443.
21. A. Yazawa: *Erzmetall,* 1977, vol. 30, p. 511.
22. A. Yazawa and M. Eguchi: *Extractive Metallurgy of Copper,* J. C. Yannopoulos and J. C. Agarwal, eds., p. 3, AIME, NY, 1976.
23. R. Schuhmann, Jr., Pei-cheh Chen, P. Palanisamy, and D. H. R. Sarma: *Met. Trans. B,* 1976, vol. 7B, p. 95.
24. A. G. Matyas and P. J. Mackey: *J. Metals,* 1976, vol. 28.
25. A. Yazawa and A. Gubčova: *Trans. TMS-AIME, 1967,* vol. 239, p. 2004.
26. A. Yazawa and T. Okura: *Bull. Res. Inst. Miner. Dress. Metall. Tohoku Univ.,* 1978, vol. 34, p. 169.
27. T. F. Remen, V. L. Kheifets, and S. E. Vaisburd: Iv. *VUZ, Zvetnaya Metall.,* 1961, no. 6, p. 58.
28. M. D. Head, V. A. Englesakis, B. C. Pearson, and D. H. Wilkinson: Paper presented at AIME Meeting, Las Vegas, Feb. 1976.
29. S. Goto: *Copper Metallurgy - Practice and Theory,* p. 23, Inst. Min. Met., 108th AIME Annual Meeting, New Orleans, Feb. 1979.
30. M. Nagamori and P. J. Mackey: *Met. Trans. B,* 1978, vol. 9B, p. 255, 567.
31. T. E. Norman: *Eng. Min. J.,* 1975, vol. 176, p. 92.
32. A. Yazawa and T. Okura: *Sulfuric Acid and Industry,* in press.
33. A. Yazawa and T. Azakami: *Can. Metall. Quart.,* 1969, vol. 8, p. 257.
34. A. Yazawa, T. Shimizu, and T. Kato: *Bull. Res. Inst. Miner. Dress. Metall., Tohoku Univ.,* 1977, vol. 33, p. 59; *Sulfuric Acid and Industry,* 1978, vol. 31, p. 97.
35. A. Yazawa and K. Itagaki: *Sulfuric Acid and Industry,* 1974, vol. 27, p. 225.
36. R. Kola: *Erzmetall,* vol. 30, p. 559.
37. I. Iwasaki: *Min. Sci. Eng.,* 1972, vol. 4, p. 14.
38. O. Kubaschewski, E. LL. Evans, and C. B. Alcock: *Metallurgical Thermochemistry,* 4th ed., Pergamon., 1967.
39. C. Rampacek, W. A. McKinney, and P. T. Waddleton: U. S. Bur. Mines, RI 5501, 1959.
40. K. Yokoyama, K. Tozawa and A. Yazawa: *Bull. Res. Inst. Miner. Dress. Metall., Tohoku Univ.,* 1975, vol. 31, p. 148.
41. M. Rey: *Trans. Inst. Min. Metall.,* 1967, vol. 76, p. C101; M. Rey, V. Formanek, P. Blanquet, and A. M. Rousseau: Paper presented at 101st AIME Annual Meeting, TMS, 1972.